A First Look at Differential Rotation in Kepler Open Clusters NGC 6811 (1 Gyr) and NGC 6819 (2.5 Gyr)

Steven H. Saar[1], **Søren Meibom**[1], **Josè-Dias do Nascimento**[1,2]

[1]*Smithsonian Astrophysical Observatory, 60 Garden St. Cambridge, MA USA 02138*

[2]*Universidade Federal do Rio Grande do Norte, UFRN, Dep. de Fisica Teorica e Experimental, DFTE Natal, Brazil*

Abstract.   Open clusters are ideal targets for controlled studies of stellar properties, since members are coeval and have the same abundances. We present the first results of measurements of surface differential rotation (SDR) in two clusters of different ages in the Kepler field. We compare results for single stars over a range of masses and rotation rates, and compare and contrast these with previous results for single and binary stars. All of these properties are found to have an effect on the average SDR rate.

1.   Introduction

Differential rotation is believed a critical component of cycling dynamos (e.g., $\alpha\Omega$ type), yet until recently, there were relatively few observations of SDR. The advent of high precision space missions like Corot and Kepler is changing this. There is concern though, that without detailed knowledge of the target stars (binarity, convection zone depth), interpretation of SDR can become muddled (Saar 2011). We measure SDR in Kepler open clusters for stars with well-determined properties (e.g., Meibom et al. 2011; Janes et al. 2013; Sandquist et al. 2013).

2.   Data and Analysis

The pipeline PDC-MAP data is carefully adjusted at data gaps to insure a smoothly varying signal. Trial fits with four sinusoids to the data pre- and post-gap are matched across gaps
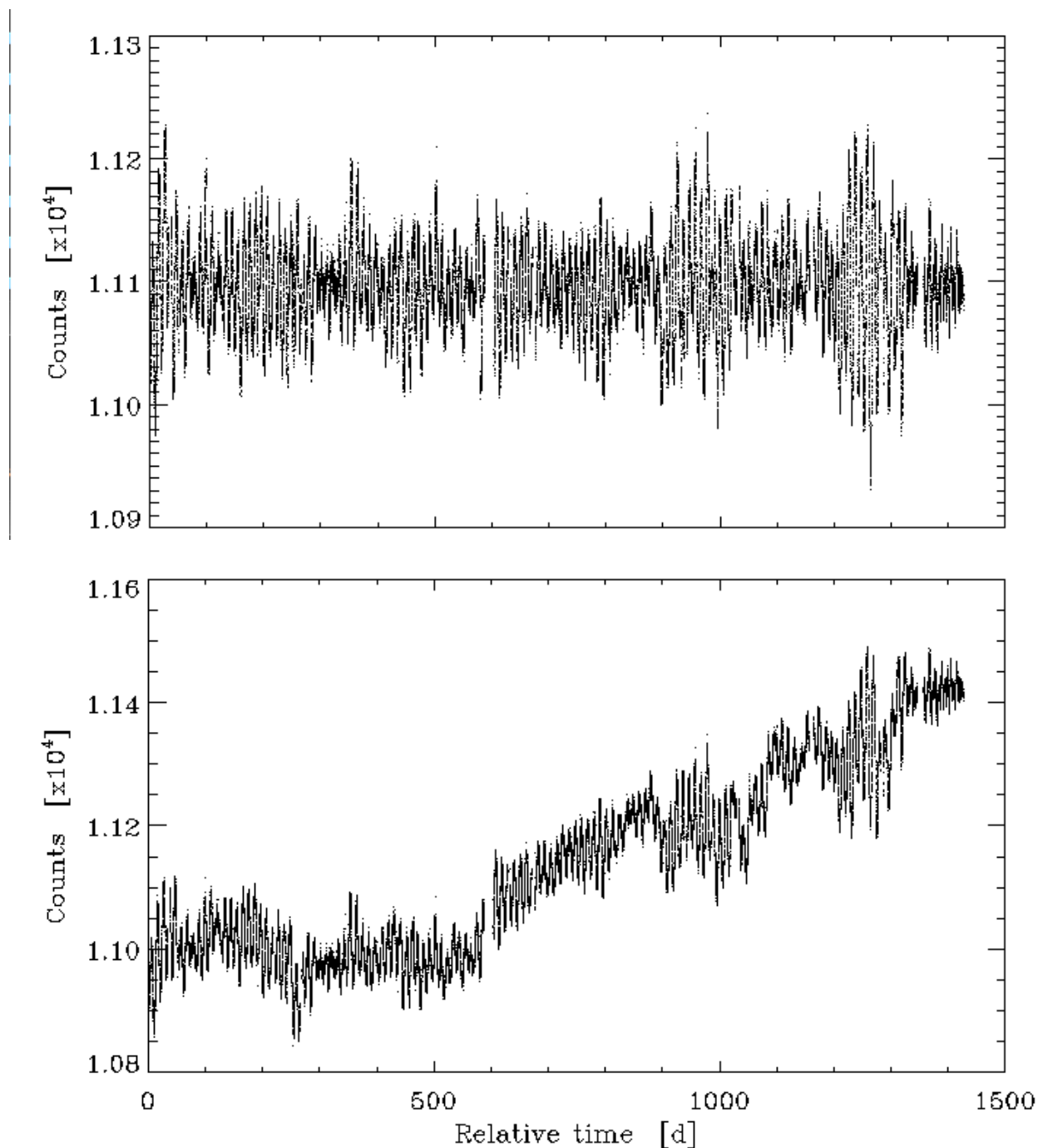
Figure .1: Kepler data for a late F star in NGC 6811, showing our post-pipeline adjustment process. Top: the quarterly data has been adjusted to a constant median value (by quarter), which removes the largest offsets. Bottom: At each significant data gap (>0.2 day) we fit the sum of four sinusoids to data just before and after the gap. Minimizing the gradient change at the intersection of these two fits is used to estimate the adjustment of the data after the gap.

to minimize gradient changes (Fig. 1). Minimizing the gradient change at the intersection of these two fits is used to estimate the adjustment of the data after the gap.

We employ two main analysis methods: wavelet, and a sliding window, floating mean Lomb-Scargle (L-S) periodogram (Scargle 1982). We focus here on results from the latter, though the former yields similar results. Each method has advantages and disadvantages: the periodogram deals better with data gaps, while the wavelet can better capture variable amplitude signals (Fig. 2).
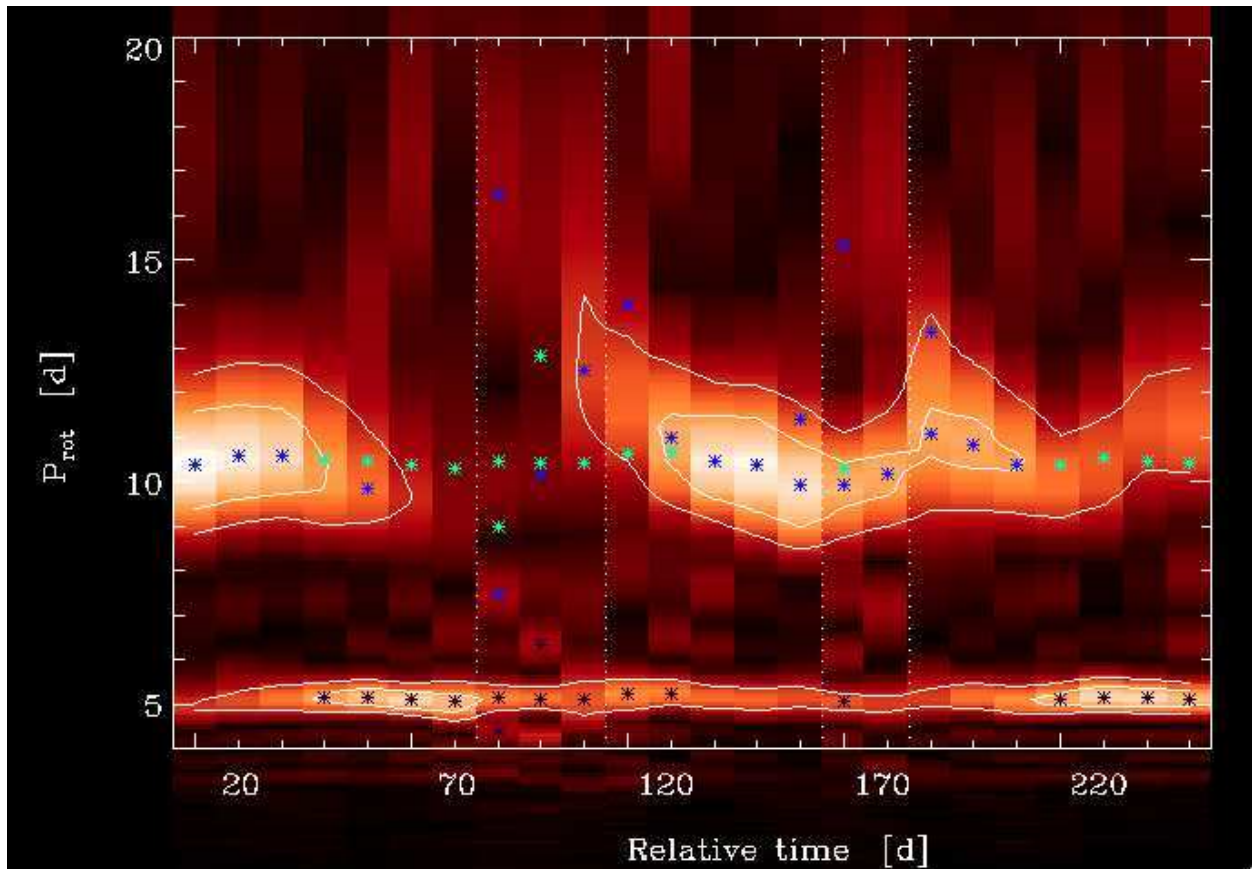
Figure .2: Expansion of part of a L-S analysis; non-aliased P_{rot} (blue *) are marked. Period doubling due to two dominant active regions is clearly seen at times (black *); these P_{rot} are replotted at twice their nominal values (green *). A dominant P_{rot} period $\sim$10.5 days is seen, while a range of weaker P_{rot} range from $\sim$9 to $\sim$13 days is also evident. Some of the apparent P_{rot} are due to higher frequency components of longer term variations. Dotted lines indicate zones where data gaps may affect the results.

Here, the window lengths chosen were 40 days (NGC 6819) and 32 days (NGC 6811), respectively, roughly 3 to 5$\times P_{rot}$ (depending on mass). The window was stepped by 10% of its length, and the periodogram recomputed. The strongest periodogram peaks can be tested individually to see if they are window aliases by comparing the observed spectrum with periodograms of pure sinusoids time-sampled identically. Periods close to the main

$P_{\rm rot}$ signal, and those close to $P_{\rm rot}$ /2 (likely due to two active longitudes) and of sufficient amplitude (log FAP < -6, where FAP is the L-S false alarm probability; Scargle 1982) are accepted as "real". Periods found in/near larger data gaps are treated with caution and rejected or given lower weight. Following the arguments of Saar (2009, 2011), we concentrate on single stars, $\sim$F5 and later. Preliminary results for a dozen selected stars spanning a range of mass ($\sim$F5 to K4) in both clusters are shown in Figs 3 and 4.
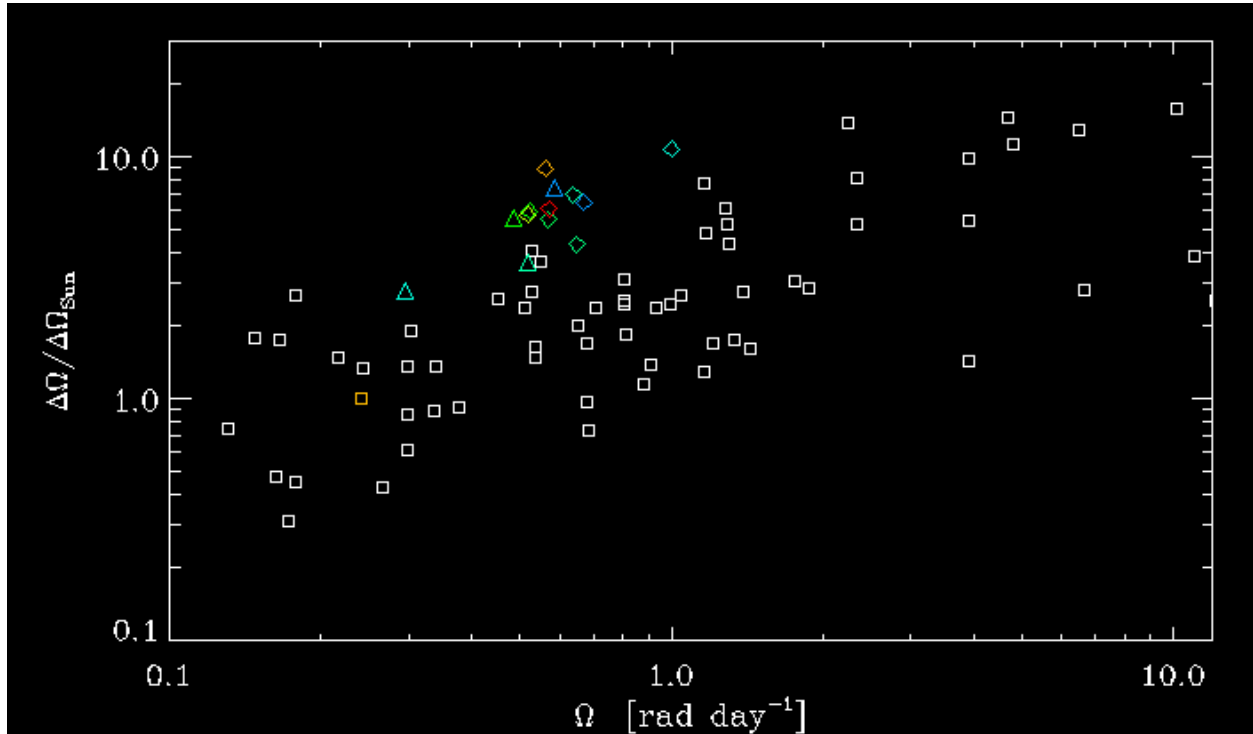
Figure .3: Differential rotation $\Delta\Omega = 2\pi(1/P_{\rm min} - 1/P_{\rm max})$ values normalized to the solar value vs. rotational frequency Ω. Here, older data (from Saar 2011, mostly from Ca II HK and photometry; e.g., Donahue et al 1996) are squares (with sun in yellow), and cluster stars are diamonds (NGC 6811) or triangles (6819). The colors indicate relative $T_{\rm eff}$, with F5 stars dark blue, through G stars (green) to K stars (orange and red). The Kepler stars show larger $\Delta\Omega$ for their rotation rates, though follow the basic trend ($\Delta\Omega \propto \Omega$).

3.   Results and Future Work

Our results are necessarily tentative, since we have only analyzed a dozen stars in detail. So far however:

The $\Delta P_{\rm rot}$ values found (Figs. 3, 4) are consistent with previous values (Donahue et al. 1996; Saar 2011), though somewhat higher at the same rotation rates. This is likely because Kepler allows us to see smaller starspots and probe a wider range of latitudes than ground-based methods (all are lower limits to the true $\Delta P_{\rm rot}$ values). We note that the apparent
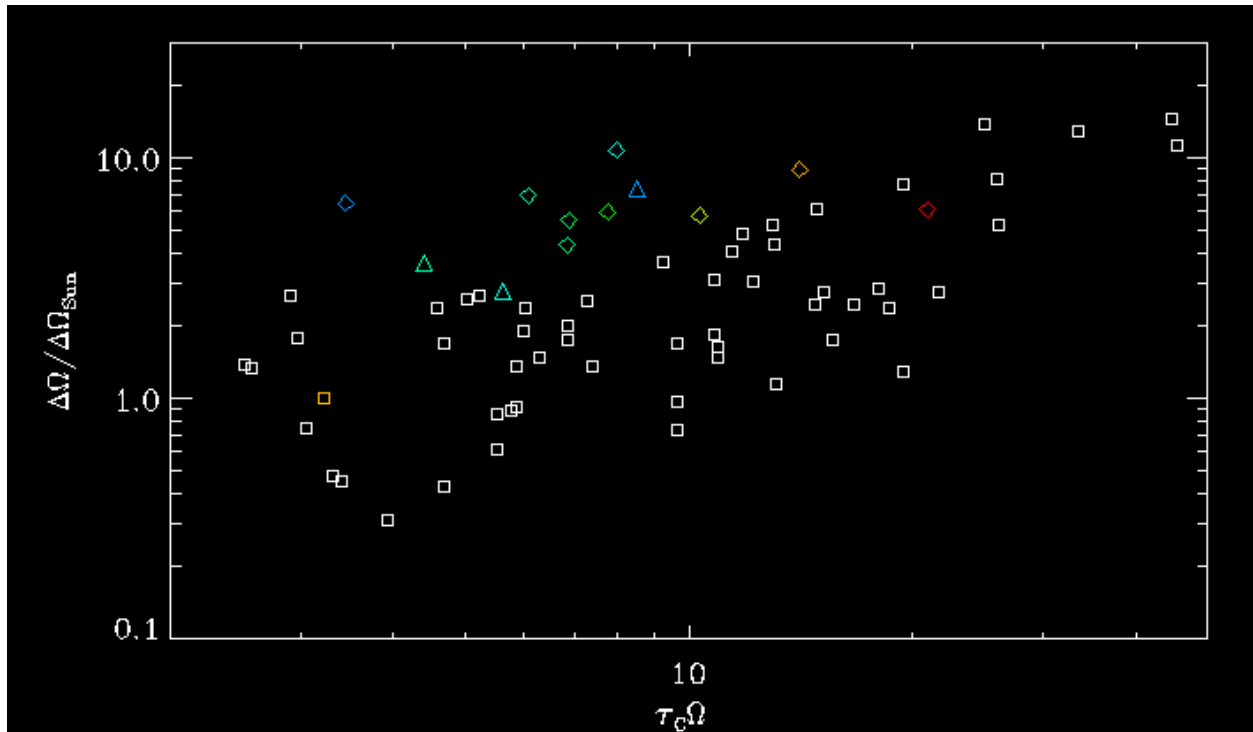
Figure .4: Differential rotation $\Delta\Omega$ values normalized to the solar value vs. inverse Rossby number $\mathrm{Ro}^{-1} = \tau_C\Omega$ (convective turnover time τ_C from Gunn et al 1998). Symbols as in Fig. 3. Again, the Kepler stars show larger $\Delta\Omega$ for their rotation rates (perhaps more noticeable here), though follow the basic trend ($\Delta\Omega \propto \mathrm{Ro}^{-1}$).

disagreement between $\Delta\Omega$ increasing with Ω seen here, and the very weak dependence of $\Delta\Omega$ on rotation seen by some others (Barnes et al. 2005; Reinhold et al. 2013, e.g.,) is likely due to the differing stellar samples studied. Both Barnes et al. (2005) and Reinhold et al. (2013) do not exclude binaries, which appear to have systematicaly lower $\Delta\Omega$ and a weaker Ω dependence.

The Neither Ω nor Ro^{-1} seem strongly preferred as a rotational diagnostic with the data studied here; clear mass dependence is see in more rapid rotators however (Saar 2009, 2011), suggesting Ro^{-1} may ultimately be superior.

The fairly wide dispersion of results can be explained a range of inclination angles i, and the limited time series studied. If these stars have solar-like magnetic cycles, they will have a dominant active region latitude (and hence measured P_{rot}) at any given time. With only a few years worth of data, we will therefore sample only a small part of the full ΔP_{rot} range the star would exhibit over its cycle.

There may be a trend towards increasing active region decay timescales (as measured by the decay of the stronger periodogram signals) with decreasing mass. This might be due to lower turbulent/granular velocities at cooler T_{eff}, which reduces convective erosion of magnetic flux concentrations. Cooler stars also tend to have larger photometric amplitudes, which suggests larger flux concentrations and/or more clumpy, asymmetric distributions.

Either of these would also lead to larger structures, and thus longer decay timescales, enhancing the T_{eff} trend, since the erosion time scales roughly as the ratio of the spot perimeter to its area, or $\approx 1/r$ where r is the spot radius.

The next step in our study will be analyze the full dataset of ~ 200 certain and candidate single cluster members, which will test these above results and permit more robust conclusions. Future work planned includes experimenting with "gapped" wavelet methods (e.g., Frick et al. 1997), which should combine the best features of the L-S and traditional wavelet analyses), systematic examination of active region decay timescales, study of binaries and evolved stars, and detailed tests of the methods against computed models (J. Llama 2014, private comm.) to check how well they recover the correct $\Delta\Omega$.

References

Barnes, J. R., Collier Cameron, A., Donati, J.-F., et al. 2005, MNRAS, 357, L1

Donahue, R. A., Saar, S. H., & Baliunas, S. L. 1996, ApJ, 466, 384

Frick, P., Baliunas, S. L., Galyagin, D., Sokoloff, D., & Soon, W. 1997, ApJ, 483, 426

Gunn, A. G., Mitrou, C. K., & Doyle, J. G. 1998, MNRAS, 296, 150

Janes, K., Barnes, S. A., Meibom, S., & Hoq, S. 2013, AJ, 145, 7

Meibom, S., Barnes, S. A., Latham, D. W., et al. 2011, ApJ, 733, L9

Reinhold, T., Reiners, A., & Basri, G. 2013, A&A, 560, A4

Saar, S. H. 2009, Solar-Stellar Dynamos as Revealed by Helio- and Asteroseismology: GONG 2008/SOHO 21, 416, 375

Saar, S. H. 2011, IAU Symposium, 273, 61

Sandquist, E. L., Mathieu, R. D., Brogaard, K., et al. 2013, ApJ, 762, 58

Scargle, J. D. 1982, ApJ, 263, 835